Low-titanium clinopyroxene composition of Nidar ophiolite gabbros, southeastern Ladakh Himalaya, India: implications to geotectonic setting

Ranjit Nayak[1,2,*] and Debasis Pal[1]

[1]Department of Earth and Atmospheric Sciences,
National Institute of Technology, Rourkela 769 008, India
[2]Department of Applied Geology, School of Applied Natural Science,
Adama Science and Technology University, 18888 Adama, Ethiopia

The Nidar ophiolite complex is one of the well-preserved ophiolite sequences of the Indus Tsangpo Suture Zone (ITSZ) towards the southeastern part of Ladakh Himalaya, India. This study presents petrography and clinopyroxene mineral chemistry of gabbroic rocks from the Nidar ophiolite. These gabbros are massive, essentially composed of plagioclase and clinopyroxene with minor amounts of olivine, orthopyroxene, hornblende and magnetite. The clinopyroxenes are very low in TiO_2 (0.05–0.77 wt%) and Na_2O (0.12–0.85 wt%) but rich in SiO_2 (52–55 wt%). It is observed that there is a wide variation of CaO (12.26–23.88 wt%) and in the Wo–En–Fs ternary diagram, clinopyroxene shows augitic to diopside compositional variation. These low-titanium clinopyroxenes are inferred to be tholeiitic in nature with an island-arc boninitic affinities.

Keywords: Gabbro, island-arc tholeiite, Ladakh Himalaya, low-Ti clinopyroxene, Nidar ophiolite.

THE compositional variation of clinopyroxene depends on the magma types related to the tectonic setting of the ophiolite sequences[1]. The high-titanium clinopyroxenes are associated with the mid-ocean ridge and back-arc/marginal sea magmatism. The low-titanium (Ti) clinopyroxenes are associated with the island arc and boninite magmatism above the subduction zone. The aluminium (Al) and Ti concentration in clinopyroxenes generally increases from tholeiitic to per-alkaline magma series, and the activity of silica controls such elemental distribution during the crystallization of magma[2,3]. Clinopyroxenes crystallized from iron (Fe)-depleted magma will have higher Ti content[4]. Earlier studies have shown that the clinopyroxene mineral chemistry can be used as an alternative tool for interpreting magmatic affinities and palaeo-geodynamic setting of ophiolites[1,4–16].

The magmatic signatures of clinopyroxenes usually remain unaltered even in metasomatized rocks[1,4,17]. Such behaviour of clinopyroxenes allows us to characterize the magmatic affinities in different tectonic settings based on statistical studies of mineral chemistry along with different discrimination plots[1,18]. Though extensive geochemical data are available on gabbros and associated rocks of the Nidar ophiolite[19,20], less emphasis was given on mineral chemistry to understand the genesis and tectonic setting of the host mafic rocks. Clinopyroxene is a common mineral found in mafic rocks, and preserves vital information about the parental magma and mantle source compositions[21–23]. Therefore, the main objective of the present study was to decipher the petrogenesis of gabbros and interpret the geodynamic setting of Nidar ophiolite based on the mineral chemistry of clinopyroxenes. Further, we compared our results with the available data of other Neo-Tethyan ophiolites.

The Nidar ophiolite is sandwiched between Tso Morari crystalline complex towards the south and Indus Formation towards the north (Figure 1). The total thickness of Nidar ophiolite varies from 3 to 12 km (ref. 24) with a maximum width of 12 km along the Nidar valley[25]. The Nidar ophiolite is a part of the Indus Suture Zone (Figure 1 *c*), characterized by ophiolites and ophiolite mélanges all along its length from Nanga Parbat to Namche Barwa[26]. The Nidar ophiolite complex can be subdivided into three litho-units[25,27–29]. The ultramafics at the bottom, followed by mafic and subsequently the volcanic units and pelagic sediments, including chert and limestone at the top. The ultramafic unit mainly consists of peridotites (harzburgite, lherzolite and dunite) with subordinate amount of chromitite and pyroxenite veins. Chromitites occur as thin parallel veins with variable thickness (1–100 cm) within the basal dunite[24,29]. Massive and isotropic gabbros are well exposed in the northwestern part of Nidar village. Well-preserved sills and dykes of plagiogranites within the gabbro unit are observed near the Shyrok stream (Figure 2 *a*). Occasionally, the gabbros also exhibit compositional layering (Figure 2 *b*). Pillow lavas from the topmost unit display a concordant association with the gabbros and are superimposed by a volcano-sedimentary unit comprising basaltic to andesitic flows, limestone, shale, green chert, siltstone and jasperite[20,29,30].

The Nidar ophiolite gabbros are fine- to medium-grained, mesocratic and massive in hand specimen. They are essentially composed of plagioclase and clinopyroxene with minor amounts of olivine, orthopyroxene, hornblende and magnetite, with an intergranular and ophitic to subophitic textural relationship. The gabbro samples were metamorphosed to some extent, but the primary magmatic phases are still preserved (Figure 2 *c*). Plagioclase is mostly subhedral lath-shaped and occurs as phenocrysts set within the groundmass of plagioclase, pyroxene, hornblende and opaque minerals. Saussuritization is more commonly observed along the grain boundary. Occasionally, phenocrysts of plagioclase exhibit albite twinning and zoning (Figure 2 *c*). Clinopyroxene in gabbros is subhedral to anhedral in nature and displays panidiomorphic to allotriomorphic texture (Figure 2 *d*). It

*For correspondence. (e-mail: nayak.ranjit213@gmail.com)

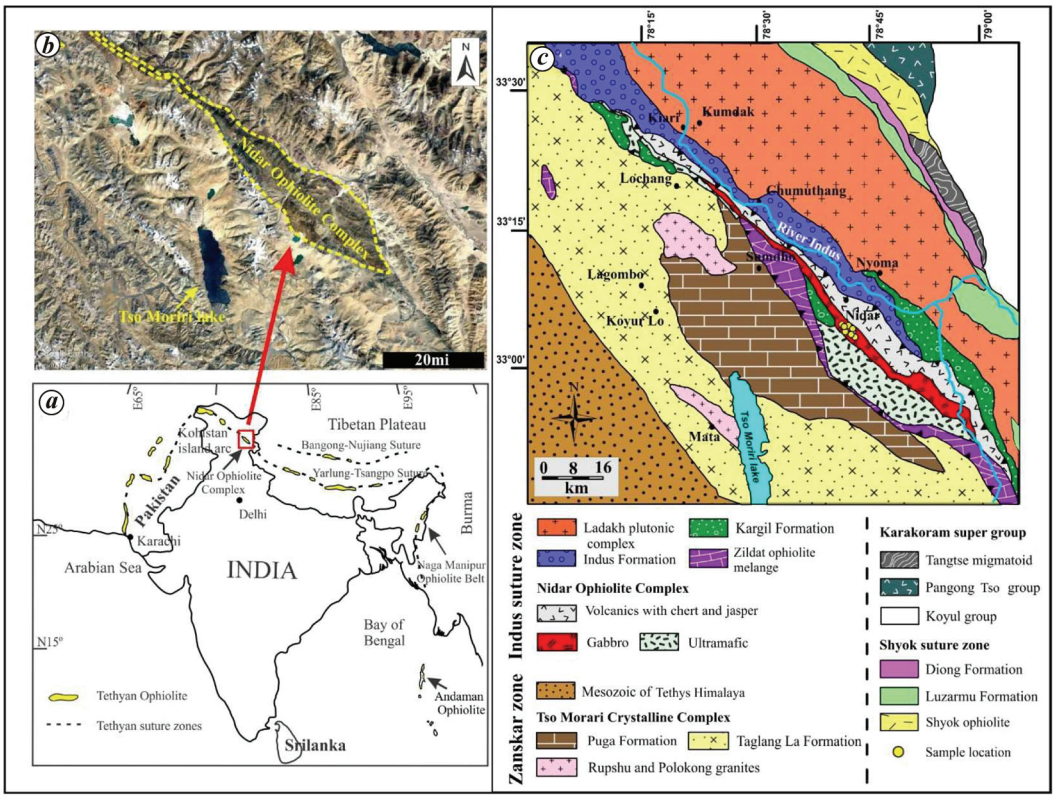

Figure 1. ***a***, Map of India showing spatial distribution of ophiolites in and around the Indian sub-continent and Tibetan plateau. ***b***, Satellite view of the Nidar ophiolite complex, southeastern ladakh, India. ***c***, Geological map of the Nidar ophiolite and surronding areas with distinct lithologies.

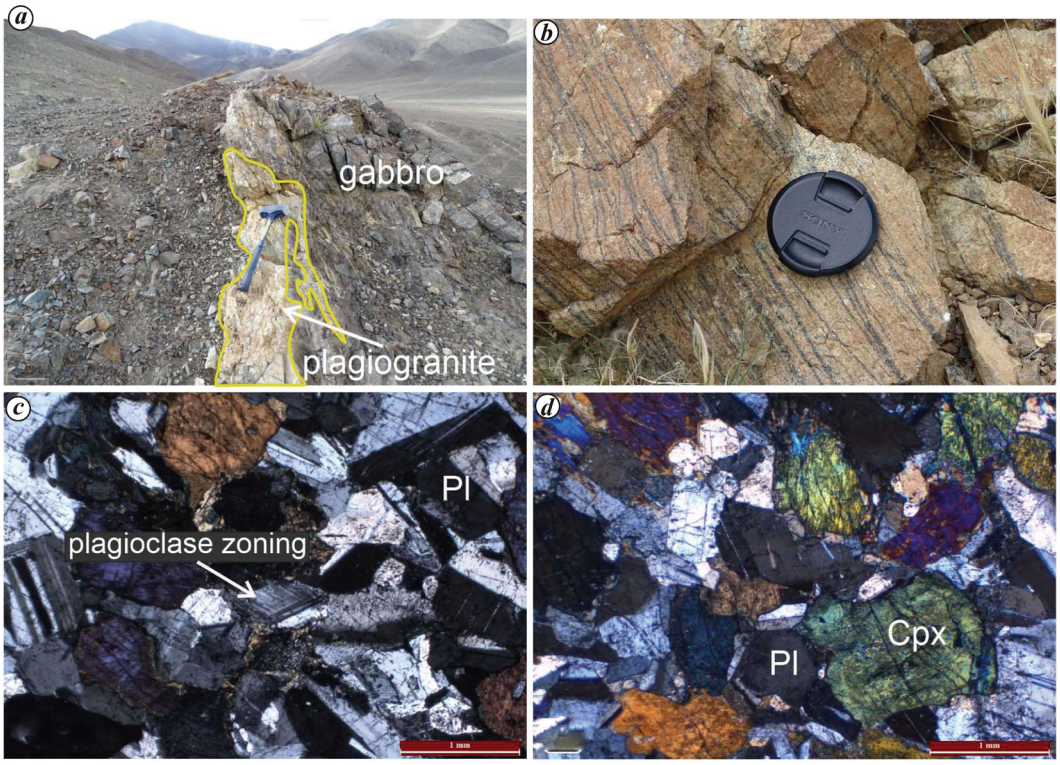

Figure 2. Field photographs: (***a***) occurrences of plagiogranite dyke in gabbros and (***b***) composition layering within the mafic sequence of the Nidar ophiolite. Photomicrographs: (***c***) laths of plagioclase with zoining and (***d***) gabbros under crossed polars showing panidiomorphic to allotriomorphic texture consisting of plagioclase and pyroxenes. Cpx, Clinopyroxene; Pl, Plagioclase.

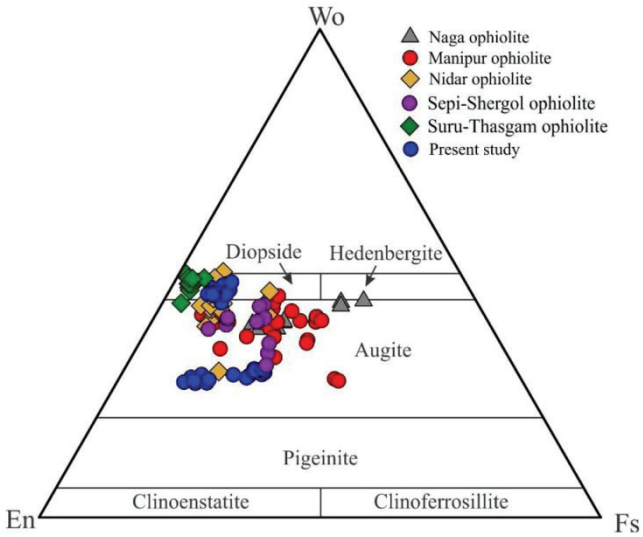

Figure 3. Trinary plot of clinopyroxene composition of the Nidar ophiolite gabbros[31]. Wo, Wollastonite; En, enstatite and Fs, Ferrosilite.

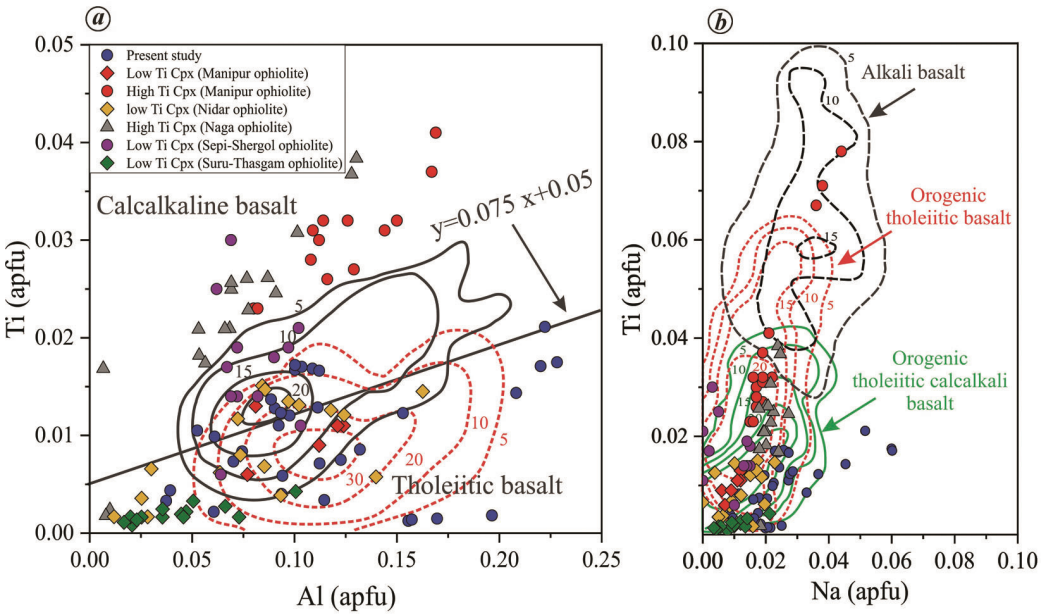

Figure 4. Discriminate diagrams of (***a***) Ti versus Al(apfu) and (***b***) Ti versus Na(apfu) of Cpx from gabbros (after Leterrier *et al.*[18]). Note the comparison between the present study and different ophiolites. The distribution of three principal basaltic families: alkali and related basalts, orogenic tholeiitic and calc-alkaline basalts is defined by computer-drawn frequency curves (the counting frequency is indicated on each contour). Data are from Manipur ophiolite[15], Nidar ophiolite[10,19], Naga ophiolite[16], Sapi–Shergol ophiolite[32] and Suru–Thasgam ophiolite[33].

has well-developed cleavage and twinning. Some of the clinopyroxene phenocrysts are either uralitized or serpentinized. Chloritization of pyroxene and/or hornblende is also noticed in few of the sections. At times it is observed that small grains of plagioclase are included in pyroxenes.

The mineral chemistry of the studied clinopyroxenes was obtained from electron microprobe analysis using Cameca SX5 operating at 15 kV and 20 nA, and beam width of 2 μm at the Indian Institute of Technology Indian School of Mines, Dhanbad. For calibrations, both natural and synthetic materials were used and the molecular proportions were calculated based on six oxygen atoms.

A total of 33 clinopyroxene data points were obtained from four Nidar ophiolite gabbro samples (Table 1). The clinopyroxene composition can be characterized by low TiO_2 (0.05–0.77 wt%) and Na_2O (0.12–0.85 wt%), with variable SiO_2 (52–55 wt%). There is a wide variation of CaO (12.26–23.88 wt%) and FeO_T (5–16 wt%), whereas

Table 1. Representative electron microprobe analyses of clinopyroxene in the gabbros of Nidar ophiolite, Ladakh Himalaya, India

Sample no.	15/N61							15/N69							15/N72				16/N110
Data points	36/1	50/1	43/1	44/1	22/1	24/1	30/1	11/1	13/1	15/1	19/1	20/1	4/1	6/1	7/1	15/1	19/1	3/1	27/1
SiO_2	54.37	53.67	54.17	52.69	53.48	52.30	52.54	52.28	54.48	52.99	52.25	51.68	51.92	52.32	51.99	52.15	51.63	52.44	55.04
TiO_2	0.14	0.27	0.21	0.12	0.45	0.05	0.05	0.40	0.32	0.12	0.77	0.46	0.35	0.62	0.61	0.47	0.60	0.62	0.08
Al_2O_3	2.15	2.82	2.16	2.58	3.55	3.56	3.87	2.12	3.10	0.85	5.18	2.06	1.39	5.13	2.51	2.57	2.30	2.32	1.40
Cr_2O_3	0.10	0.24	0.10	0.12	0.16	0.07	0.01	0.01	0.00	0.00	0.02	0.08	0.00	0.00	0.13	0.07	0.27	0.09	0.13
FeO	12.67	12.53	12.75	13.42	6.66	13.62	13.48	6.33	8.09	5.41	8.88	6.38	6.27	9.02	4.59	4.79	5.25	4.39	7.86
Fe_2O_3	2.24	2.21	2.25	2.37	1.18	2.40	2.38	1.12	1.43	0.96	1.57	1.13	1.11	1.59	0.81	0.84	0.93	0.78	1.39
MnO	0.26	0.16	0.30	0.34	0.23	0.14	0.19	0.20	0.18	0.27	0.25	0.24	0.16	0.16	0.15	0.16	0.06	0.11	0.11
MgO	14.61	15.31	14.80	14.10	19.52	13.76	13.99	15.87	19.28	15.35	17.75	14.89	14.74	17.73	16.25	16.22	16.18	16.54	19.15
CaO	13.30	12.50	13.11	12.58	12.47	12.83	13.18	21.31	12.61	23.41	12.51	22.55	23.75	12.51	22.60	22.33	22.19	22.35	12.78
Na_2O	0.12	0.25	0.12	0.13	0.52	0.30	0.29	0.38	0.47	0.23	0.73	0.40	0.31	0.85	0.38	0.40	0.34	0.36	0.26
Total	99.97	99.99	99.98	98.50	98.25	99.03	99.97	100.01	99.96	99.59	99.95	99.87	100.00	99.95	100.02	100.00	99.75	100.00	98.19
O = 6																			
Si	2.01	1.98	2.00	1.99	1.95	1.96	1.95	1.93	1.97	1.97	1.90	1.92	1.93	1.90	1.91	1.92	1.91	1.92	2.02
Al^{IV}	0.00	0.02	0.00	0.01	0.05	0.04	0.05	0.07	0.03	0.03	0.10	0.08	0.06	0.10	0.09	0.08	0.09	0.08	0.00
Al^{VI}	0.09	0.10	0.09	0.10	0.11	0.12	0.12	0.02	0.10	0.00	0.12	0.01	0.00	0.13	0.02	0.03	0.01	0.02	0.06
Ti	0.00	0.01	0.01	0.00	0.01	0.00	0.00	0.01	0.01	0.00	0.02	0.01	0.01	0.02	0.02	0.01	0.02	0.02	0.00
Cr	0.00	0.01	0.00	0.00	0.00	0.00	0.00	0.00	0.00	0.00	0.00	0.00	0.00	0.00	0.00	0.00	0.01	0.00	0.00
Fe^{2+}	0.39	0.39	0.39	0.42	0.20	0.43	0.42	0.20	0.24	0.17	0.27	0.20	0.20	0.27	0.14	0.15	0.16	0.13	0.24
Fe^{3+}	0.06	0.06	0.06	0.07	0.03	0.07	0.07	0.03	0.04	0.03	0.04	0.03	0.03	0.04	0.02	0.02	0.03	0.02	0.04
Mn	0.01	0.00	0.01	0.01	0.01	0.00	0.01	0.01	0.01	0.01	0.01	0.01	0.01	0.00	0.00	0.00	0.00	0.00	0.00
Mg	0.81	0.84	0.82	0.79	1.06	0.77	0.78	0.87	1.04	0.85	0.96	0.83	0.82	0.96	0.89	0.89	0.89	0.90	1.05
Ca	0.53	0.49	0.52	0.51	0.49	0.52	0.53	0.84	0.49	0.93	0.49	0.90	0.95	0.49	0.89	0.88	0.88	0.88	0.50
Na	0.01	0.02	0.01	0.01	0.04	0.02	0.02	0.03	0.03	0.02	0.05	0.03	0.02	0.06	0.03	0.03	0.02	0.03	0.02
$Mg^{\#}$	0.67	0.69	0.67	0.65	0.84	0.64	0.65	0.82	0.81	0.83	0.78	0.81	0.81	0.78	0.86	0.86	0.85	0.87	0.81
Wo	30.56	28.68	30.03	29.48	27.81	30.12	30.53	44.09	27.56	47.77	28.34	46.74	48.31	28.29	46.32	45.91	45.47	45.80	28.04
En	46.71	48.88	47.18	45.98	60.59	44.93	45.10	45.69	58.64	43.60	55.95	42.94	41.73	55.79	46.34	46.41	46.13	47.17	58.49
Fs	22.73	22.44	22.80	24.55	11.60	24.95	24.37	10.23	13.80	8.63	15.71	10.32	9.96	15.92	7.34	7.68	8.40	7.03	13.47

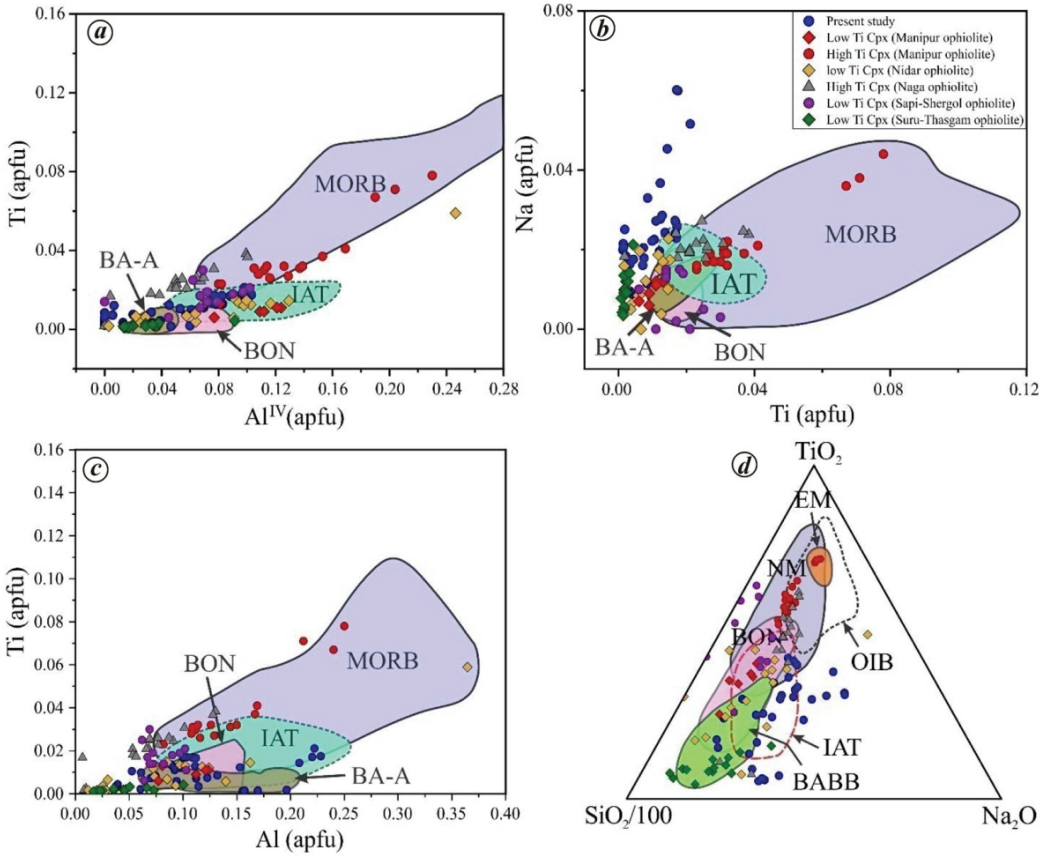

Figure 5. Tectonic discriminate diagrams of clinoproxene compositions: ***a***, Al^{IV} versus Ti(apfu); ***b***, Ti versus Na(apfu); ***c***, Al versus Ti(apfu). ***d***, Ternary discriminate TiO_2–SiO_2/100–Na_2O diagram of clinopyroxenes from the gabrros of Nidar ophiolite[1]. EM, Enriched mid-ocean ridge basalt; NM: Normal mid-ocean ridge basalt; OIB, Ocean island basalt; BON, Boninite; IAT, Island-arc tholeiite and BABB, Back-arc basin basalt.

variation of Mg# [Mg/(Mg + Fe^{2+})] ranges from 0.64 to 0.87. The ternary diagram[31] of Wo–En–Fs indicates that the clinopyroxenes are augitic to diopside in composition (Figure 3). There is slight compositional variation between core and rim in some clinopyroxene grains with regard to TiO_2 and Al_2O_3 content. These are classified as low-Ti (<0.025 apfu)[1] clinopyroxenes based on the variable content of TiO_2, SiO_2 and Na_2O (wt%).

Leterrier *et al.*[18] have proposed that the elements like Na, Ti, Cr, Ca and Al in clinopyroxene can be used to discriminate the parental magmas in different tectonic settings. Beccaluva *et al.*[1] have grouped the Ti content in clinopyroxene as high-Ti, low-Ti and very low-Ti ophiolites, suggesting that the high-Ti ophiolites occur at mid-ocean ridges and marginal basins. The low-Ti and very low-Ti types are generated at supra-subduction zone settings. The activity of an element in clinopyroxene crystallizing from a liquid could be explained by the partition coefficient factor (K_D). Consequently, chemical variation of the magma will reflect in the composition of clinopyroxene, mainly for the elements readily combined in their matrix. For example, the orogenic basalts (island-arc tholeiites and basaltic andesite, calc-alkali basalts from active continental margins and shoshonitic basalts) are depleted in Ti and Cr. The tholeiites and transitional basalts from oceanic ridges, continental rift, back-arc basin and passive continental margins are enriched in Ti and Na, but are Si-deficient when compared with other types of basalts[18]. The bivariate diagrams (Figure 4 *a* and *b*)[18] illustrate the comparison between low-Ti cpx from Nidar ophiolite and other Neo-Tethyan ophiolites (Manipur ophiolite[15], Nidar ophiolite[10,19], Naga ophiolite[16], Sapi–Shergol ophiolite[32], Suru–Thasgam ophiolite)[33]. Our results are consistent with the low-Ti which signifies orogenic tholeiitic calcalkali basalts.

The clinopyroxene compositions like Al_2O_3, Na_2O and TiO_2 in mafic rocks are primarily controlled by the composition of magma and specifically by the activity of SiO_2 and alkalinity[34]. However, it may have a limited influence on the physical conditions of crystallization. The magmatic processes that are responsible for the generation of the ophiolite complexes regulate the geochemical and petrological signatures, depending on the geodynamic settings of their development[35]. The high Mg content in these clinopyroxenes is consistent with pyroxene compositions reported in other ophiolite complexes and Island

Arcs[36]. The observed high SiO_2 and low Ti content correspond to basalts produced in orogenic settings. The discriminate diagrams using Ti, Si, Al and Na elements in clinopyroxene deduce the more distinct classification of magma types[1]. In the bivariate diagram Ti versus Al^{IV} (apfu), the low-Ti clinopyroxenes of Nidar ophiolite fall in the compositional field of island-arc tholeiite (IAT; Figure 5 *a*). Similarly, plots related to Na, Ti and Al also suggest the signature of IAT (Figure 5 *b* and *c*). The TiO_2–SiO_2/100–Na_2O diagram exhibits well within magmatic series of IAT field (Figure 5 *d*)[1]. Thus, it can be inferred that the Nidar ophiolite with low-Ti cpx is consistent with the adjoining ophiolites and reflects supra-subduction setting of boninitic affinity.

1. Beccaluva, L., Macciotta, G., Piccardo, G. B. and Zeda, O., Clinopyroxene composition of ophiolite basalts as petrogenetic indicator. *Chem. Geol.*, 1989, **77**, 165–182.
2. Le Bas, M. J., The role of aluminium in igneous clinopyroxenes with relation to their parentage. *Am. J. Sci.*, 1962, **260**, 267–288.
3. Kushiro, I., Si–Al relation in clinopyroxenes from igneous rocks. *Am. J. Sci.*, 1960, **258**, 548–554.
4. Nisbet, E. G. and Pearce, J. A., Clinopyroxene composition in mafic lavas from different tectonic settings. *Contrib. Mineral. Petrol.*, 1977, **63**, 149–160.
5. Hebert, R. and Laurent, R., Mineral chemistry of the plutonic section of the Troodos ophiolite: new constraints for genesis of arc-related ophiolites. In *Troodos 1987 Ophiolites and Oceanic Lithosphere* (eds Malpas, G. J. and Moores, E. M.), 1987, pp. 149–163.
6. Capedri, S. and Venturelli, G., Clinopyroxene composition of ophiolitic metabasalts in the Mediterranean area. *Earth Planet Sci. Lett.*, 1979, **3**, 61–73.
7. Smith, D. and Lindsley, D. H., Stable and metastable augite crystallization trends in a single basalt flow. *Am. Mineral.*, 1971, **56**, 225–233.
8. Deer, W. A., Howie, R. A. and Zussmann, J., In *Rock-Forming Minerals: Single-chain Silicates*, V. 2A, Wiley, New York, USA, 1978, p. 528.
9. Papike, J. J. and White, C., Pyroxenes from the planetary basalts: characterization of 'other' than quadrilateral components. *Geophys. Res. Lett.*, 1979, **6**, 913–916.
10. Arndt, N. T. and Fleet, M. E., Stable and metastable pyroxene crystallization in layered komatiite lava flows. *Am. Mineral.*, 1979, **64**, 856–864.
11. Coish, R. A. and Taylor, L. A., The effects of cooling rate on texture and pyroxene chemistry in DSDP Leg 34 basalt: a microprobe study. *Earth Planet. Sci. Lett.*, 1979, **42**, 389–398.
12. Gamble, R. P. and Taylor, L. A., Crystal/liquid partitioning in augite: effects of cooling rate. *Earth Planet. Sci. Lett.*, 1980, **47**, 21–33.
13. Cameron, M. and Papike, J. J., Structural and chemical variations in pyroxenes. *Am. Mineral.*, 1981, **66**, 1–50.
14. Yaliniz, K. M. and Göncüoğlu, M. C., Clinopyroxene compositions of the isotropic gabbros from the Sarıkaraman Ophiolite: new evidence on supra-subduction zone type magma genesis in Central Anatolia. *Turkish J. Earth Sci.*, 2000, **8**(2–3), 103–112.
15. Ovung, T. N., Ray, J., Ghosh, B., Koeberl, C., Topa, D. and Paul, M., Clinopyroxene composition of volcanics from the Manipur Ophiolite, Northeastern India: implications to geodynamic setting. *Int. J. Earth Sci.*, 2018, **107**(4), 1215–1229.
16. Nayak, R., Rao, B. V. and Merangsoba, Clinopyroxene compositions of the gabbro from the Naga Ophiolite belt: new evidence on supra-subduction type magma genesis. *J. Appl. Geochem.*, 2013, **15**(1), 61–69.
17. Fodor, R. V. and Thiede, J., Volcanic breccias from DSDP site 357: implications for the composition and origin of the Rio Grande rise. In *Initial Reports of the Deep-Sea Drilling Project* (eds Supko, K. *et al.*), 1977, vol. 39, pp. 537–543.
18. Leterrier, J., Maury, R. C., Thonon, P., Girard, D. and Marchal, M., Clinopyroxene composition as a method of identification of the magmatic affinities of paleo-volcanic series. *Earth Planet. Sci. Lett.*, 1982, **59**, 139–154.
19. Ahmad, T., Tanaka, T., Sachan, H. K., Asahara, Y., Islam, R. and Khanna, P. P., Geochemical and isotopic constraints on the age and origin of the Nidar Ophiolitic Complex, Ladakh, India: implications for the Neo-Tethyan subduction along the Indus suture zone. *Tectonophysics*, 2008, **451**(14), 206224.
20. Mahéo, G., Bertrand, H., Guillot, S., Villa, I. M., Keller, F. and Capiez, P., The South Ladakh ophiolites (NW Himalaya, India) and intra-oceanic tholeiitic arc origin with implications for the closure of the Neo-Tethys. *Chem. Geol.*, 2004, **203**, 273–303.
21. Miyazaki, T. *et al.*, Clinopyroxene and bulk rock Sr–Nd–Hf–Pb isotope compositions of Raivavae ocean island basalts: does clinopyroxene record early stage magma chamber processes? *Chem. Geol.*, 2017, **482**, 18–31.
22. Batki, A. *et al.*, Insights into the evolution of an alkaline magmatic system: an *in situ* trace element study of clinopyroxenes from the Ditrău Alkaline Massif, Romania. *Lithos*, 2018, **300–301**, 51–71.
23. Li, X. *et al.*, Integrated major and trace element study of clinopyroxene in basic, intermediate and acidic volcanic rocks from the middle Okinawa Trough: insights into petrogenesis and the influence of subduction component. *Lithos*, 2020, **352–353**, 105320.
24. Nayak, R., Pal, D. and Chinnasamy, S. S., High-Cr chromitites of the Nidar Ophiolite Complex, northern India: petrogenesis and tectonic implications. *Ore Geol. Rev.*, 2020, **129**, 103942.
25. Nayak, R. and Maibam, B., Petrological study of spinel peridotites of Nidar Ophiolite, Ladakh Himalaya, India. *J. Earth Syst. Sci.*, 2020, **129**(1), 115; https://doi.org/10.1007/ s12040-019-1308-1.
26. Rao, D. R., Rai, H. and Kumar, J. S., Origin of oceanic plagiogranite in the Nidar ophiolite sequence of eastern Ladakh, India. *Curr. Sci.*, 2004, **87**, 999–1005.
27. Das, S., Mukherjee, B. K., Basu, A. R. and Sen, K., Peridotitic minerals of the Nidar ophiolite in the NW Himalaya: sourced from the depth of the mantle transition zone and above. *Geol. Soc. Spec. Publ.*, 2015, **412**(1), 271–286.
28. Das, S., Basu, A. R. and Mukherjee, B. K., *In situ* peridotitic diamond in Indus ophiolite sourced from hydrocarbon fluids in the mantle transition zone. *Geology*, 2017, **45**(8), 755–758.
29. Sachan, H. K. and Mukherjee, B. K., Genesis of chromite in ophiolites from Indus Suture Zone, Ladakh, India: evidence from mineral chemistry of solid inclusions in chromite. *Him. Geol.*, 2003, **24**, 63–74.
30. Ravikant, V., Pal, T. and Das, D., Chromites from the Nidar ophiolite and Karzok complex, Trans Himalaya, eastern Ladakh: their magmatic evolution. *J. Asian Earth Sci.*, 2004, **24**(2), 177–184.
31. Morimoto, N., Nomenclature of pyroxenes. *Mineral. Petrol.*, 1988, **39**, 55–76.
32. Bhat, I. M., Ahmad, T. and Rao, D. S., Petrology and geochemistry of mafic intrusive rocks from the Sapi-Shergol ophiolitic mélange, Indus Suture Zone, western Ladakh: constraints on petrogenesis and tectonic setting. *J. Geol.*, 2019, **127**(5), 543–566.
33. Bhat, I. M., Ahmad, T., Rao, D. S. and Rao, N. C., Petrological and geochemical characterization of the arc-related Suru–Thasgam ophiolitic slice along the Indus Suture Zone, Ladakh Himalaya. *Geol. Mag.*, 2021, 1–20.
34. Brown, G. M., Mineralogy of the basaltic rocks. In *Basalts* (eds Hess, H. H. and Poldervaart, A.), Interscience, New York, USA, 1967, pp. 103–162.

35. Dilek, Y. and Newcomb, S. (eds), Ophiolite concept and its evolution. In *Ophiolite Concept and the Evolution of Geological Thought*, Geological Society of America, Special Papers, Boulder, Colorado, 2003, no. 373, pp. 1–16.
36. De Bari, S. M. and Coleman, R. G., Examination of the deep levels of an island arc: evidence from the Tonisia ultramafic–mafic assemblage, Tonisia, Alaska. *J. Geophys. Res.*, 1989, **94**, 73–91.

ACKNOWLEDGEMENTS. R.N. thanks the Department of Science and Technology, Government of India for financial support (Fast Track Young Scientist, grant no. SR/FTP/ES-60/2014). We thank Mr Durgesh and Dr Shusanta Sarangi (Department of Applied Geology, IIT (ISM) Dhanbad) for help in EPM analyses; and Dr Sakthi Saravanan Chinnasamy (Department of Earth and Atmospheric Science, NIT, Rourkela) for laboratory facilities. We are also thankful to Prof. Krishna Kishore Osuri (Department of Earth and Atmospheric Sciences, NIT, Rourkela) for language editing. Prof. Chalapathi Rao for editorial handling and the anonymous reviewers for their valuable suggestions that helped improve the manuscript.

Received 2 March 2021; revised accepted 6 July 2021

doi: 10.18520/cs/v121/i5/685-691

Vegetative propagation of *Ulmus villosa* Brandis and *Ulmus wallichiana* Planchon: optimizing plant growth regulators and growing media on root formation in hardwood stem cuttings

Ishrat Nazir*, Vaishnu Dutt, Anup Raj, G. M. Bhat, Bilal Ahmad Bhat and Akhlaq Amin Wani

Faculty of Fisheries, Sher-e-Kashmir University of Agricultural Sciences and Technology of Kashmir (SKUAST-K), Shalimar, Srinagar 190 025, India

***Ulmus villosa* and *Ulmus wallichiana* are agroforestry tree species of the Kashmir valley, India. Low viability and less longevity of the seeds limit their propagation. The hardwood stem cuttings of both species were propagated in growing medium (soil, sand and a mixture of cocopeat : vermiculite : perlite) and treated with different indole-butyric acid (IBA) concentrations. The results showed maximum sprouting, rooting, survival, shoot length, root length, and leaf area at 2500 and 2000 ppm IBA for *U. villosa* and *U. wallichiana* respectively. Moreover, with cocopeat : vermiculite : perlite 2 : 1 : 1, significant results were observed in both the species. The interaction between planting media and IBA concentration showed significant variance.**

Keywords: Growing media, indole-butyric acid, stem cuttings, *Ulmus villosa*, *Ulmus wallichiana*, vegetation propagation.

*For correspondence. (e-mail: ishratnazir12345@gmail.com)

ELMS are common worldwide, generally distributed in the temperate regions of the Northern Hemisphere, subtropics of Central America and Southeast Asia[1]. A total of 35 species are distributed throughout the world, but only 5 are reported in the Indian subcontinent, viz. *Ulmus wallichiana*, *Ulmus villosa*, *Ulmus pumila*, *Ulmus chumlia* and *Ulmus lanceifolia*. Two species, namely *U. wallichiana* and *U. villosa* have been reported from the Kashmir valley, India, but show low regeneration in the forests due to rare seed availability[2].

Ulmus villosa Brandis is a deciduous tree popularly called marinoo in India[3]. The tree shows scattered distribution in Northwestern Himalayas and grows up to 20–30 m in height at an altitude ranging from 1200 to 2500 m amsl (ref. 4). It is considered an important agroforestry tree species, but irrespective of its multi-purpose advantages meagre research thrust has been given on the quantitative or qualitative development and mass production of the species[5].

Ulmus wallichiana Planchon, famous as Kashmiri elm, Bhutan elm or Himalayan elm, is found at elevations ranging from 800 to 3000 m amsl, distributed from Nuristan in Afghanistan, northern Pakistan and India to western Nepal. The species is widely distributed in Kashmir, especially found in Dachigam, Tangmarg, Babareshi, Pahalgam, Chandanwari and Verinag[3]. The Himalayan elm can reach up to a height of 30 m with distinct greyish-brown trunk furrowed longitudinally, broad crown region and branches grow in ascending fashion[3]. Naturally the elm tree shows sexual mode of propagation through seeds, but the seeds of *U. wallichiana* are either empty or exhibit less longevity, which results in low availability for afforestation. Like *U. villosa*, *U. wallichiana* is source of fuel, timber and is reported to have the potential to prevent and treat osteoporosis[6].

In order to overcome the propagation barrier through seed multiplication, vegetative propagation has been a thrust area in the recent past. Vegetative propagation through stem cuttings can be used to select superior varieties of *U. villosa* and *U. wallichiana* for planting. One of the critical aspects for propagation by stem cuttings is the root development process which is influenced by the plant growth regulators, especially by the root-stimulating agents. They play a crucial role in root development in difficult-to-root plants, improving rooting percentage in cuttings and decreasing rooting time[7].

The choice of rooting medium is one of the most important factors for achieving optimum rooting in the shortest time. It is important to choose the correct rooting medium to get optimum rooting in the shortest time. Peat moss is the most commonly used peat in horticulture[8]. It is reported that peat moss improves the physical characteristics of the soil, such as porosity and water-holding capacity[9].

The aim of this study was to analyse the impact of growth regulators and growing media on the rooting of *U. villosa* and *U. wallichiana* hardwood stem cuttings.